Exchange of groundwater and surface-water mediated by permafrost response to seasonal and long term air temperature variation

Shemin Ge,[1] Jeffrey McKenzie,[2] Clifford Voss,[3] and Qingbai Wu[4]

Received 28 April 2011; revised 13 June 2011; accepted 17 June 2011; published 30 July 2011.

[1] Permafrost dynamics impact hydrologic cycle processes by promoting or impeding groundwater and surface water exchange. Under seasonal and decadal air temperature variations, permafrost temperature changes control the exchanges between groundwater and surface water. A coupled heat transport and groundwater flow model, SUTRA, was modified to simulate groundwater flow and heat transport in the subsurface containing permafrost. The northern central Tibet Plateau was used as an example of model application. Modeling results show that in a yearly cycle, groundwater flow occurs in the active layer from May to October. Maximum groundwater discharge to the surface lags the maximum subsurface temperature by two months. Under an increasing air temperature scenario of 3°C per 100 years, over the initial 40-year period, the active layer thickness can increase by three-fold. Annual groundwater discharge to the surface can experience a similar three-fold increase in the same period. An implication of these modeling results is that with increased warming there will be more groundwater flow in the active layer and therefore increased groundwater discharge to rivers. However, this finding only holds if sufficient upgradient water is available to replenish the increased discharge. Otherwise, there will be an overall lowering of the water table in the recharge portion of the catchment.
Citation: Ge, S., J. McKenzie, C. Voss, and Q. Wu (2011), Exchange of groundwater and surface-water mediated by permafrost response to seasonal and long term air temperature variation, *Geophys. Res. Lett.*, *38*, L14402, doi:10.1029/2011GL047911.

1. Introduction

[2] Permafrost, defined as subsurface regions that contain perennially-frozen water, exists extensively across high latitude regions and sporadically in high altitude regions, occupying approximately 24% exposed area of the northern hemisphere [*Zhang et al.*, 2003] and less than 25% of the southern circumpolar region [*Bockheim*, 1995]. As permafrost impedes groundwater flow, it is speculated that thinning and thawing of permafrost will significantly alter water cycle processes near the earth's surface, for example, by affecting baseflow contributions to rivers or streams [*Michel*, 1994; *Yang et al.*, 2002; *Liu et al.*, 2003; *Zarnetske et al.*, 2008; *St. Jacques and Sauchyn*, 2009]. Permafrost integrity is directly affected by climatic conditions. If land surface temperatures increase, permafrost may experience warming and thawing [*Smith et al.*, 2010; *Zhao et al.*, 2010], leading to permeability increases. Consequently, groundwater discharge to surface water bodies will increase. These intensified groundwater - surface water interactions could promote transport of dissolved solids, nutrients, or carbon in the shallow subsurface [*Frey et al.*, 2007; *Walvoord and Striegl*, 2007].

[3] The 'active layer' is the supra-permafrost zone in the top few meters near the ground surface where ice forms and thaws seasonally [*Hinzman et al.*, 1991]. The lower boundary of the active layer, the permafrost table, is the top of permafrost. *Shur et al.* [2005] advocated that a transitional layer between the active layer and permafrost should be recognized and this transitional layer episodically changes its state from perennially frozen permafrost to seasonally thawed active layer. A common assumption for the permafrost temperature state is that it responds to the land surface temperature variations and that the permafrost spatial extent is governed by subsurface heat conduction. The active layer and permafrost are porous media consisting of air, solids, and water that can take the form of ice, liquid water or water vapor. Thus, heat can also be transported by advection as water and vapor move through the porous materials. This study examines the heat transport processes in the permafrost region considering both conduction and advection in flowing liquid water.

[4] As subsurface temperatures in permafrost regions change, the permeability of the active layer increases as a result of thawing or reduces as a result of freezing. Consequently, groundwater flow in the active layer and groundwater discharge to surface waters could be promoted or impeded. The objective of this study is to examine the impact of air temperature changes on permafrost temperature, active layer thickness, and groundwater discharge to the surface over seasonal and decadal time scales. A numerical modeling approach is used.

2. Background on Modeling Groundwater Flow and Heat Transport in Permafrost

[5] The theoretical basis for coupling groundwater flow to heat transport is well established and extensively applied to hydrogeological and geothermal studies [e.g., *Person et al.*, 1996; *Ingebritsen et al.*, 2006]. There are more recent applications in studying permafrost. For example, *McKenzie*

[1]Department of Geological Sciences, University of Colorado at Boulder, Boulder, Colorado, USA.
[2]Earth and Planetary Sciences, McGill University, Montreal, Quebec, Canada.
[3]U.S. Geological Survey, Menlo Park, California, USA.
[4]State Key Laboratory of Frozen Soil Engineering, Cold and Arid Regions Environmental and Engineering Research Institute, Chinese Academy of Sciences, Lanzhou, China.

0094-8276/11/2011GL047911

Table 1. Model Parameters Used in This Study

Parameter	Value	Unit
Density of water, ρ	1000	kg/m^3
Dynamic viscosity of water, μ	0.001	kg/(m s)
Dispersivity	5	m
Fitting parameter, w	0.1	
Freezing point temperature, T_L	0	°C
Gravitational acceleration	9.8	m/s^2
Latent heat of fusion, L	3.4×10^5	J/kg
Permeability, k_s	1×10^{-13}	m^2
Permeability impedance factor, Ω	5	
Minimum permeability	10^{-6} k_s	
Porosity (CM, FH), n	0.2, 0.3	
Residual water saturation, S_{wres}	0.05	
Specific heat capacity of water, C_f	4182	J/(kg °C)
Specific heat capacity of ice, C_i	2108	J/(kg °C)
Specific heat capacity of solid, C_s	840	J/(kg °C)
Thermal conductivity of water	0.6	J/(m s °C)
Thermal conductivity of solid	3.5	J/(m s °C)
Temperature gradient	3/100	°C/year
Numerical model mesh, Δx	5	m

et al. [2007] developed a coupled groundwater flow and heat transport model and simulated dynamic ice and temperature distributions in a peatland in Minnesota, USA. *Thomas et al.* [2009] presented a one-dimensional coupled heat flow, water movement, and mechanical deformation model. The emphasis of *Thomas et al.* [2009] was on ice segregation and applications to permafrost related mass movement. *Bense et al.* [2009] presented a coupled groundwater flow and heat transport model simulating reactivation of a permafrost-covered groundwater flow system in response to permafrost thawing. Their results predicted that a substantial increase in groundwater discharge to streams over the next few centuries will likely occur in response to climate warming scenarios. *Bense et al.*'s [2009] study focused on century scale changes, and the dynamics of seasonal permafrost freezing and thawing was not included. To better understand groundwater flow and heat transport processes in the active layer where most groundwater flow might be expected to occur, consideration of seasonal variations allows capturing groundwater variations within a year and more realistically simulating the physical processes in the active layer. This study focuses on the flow processes at seasonal and decadal scales.

3. Method

3.1. Modeling Basics

[6] A key factor for groundwater flow and heat transport in permafrost regions is that water undergoes phase transition between solid ice and liquid water as subsurface temperature fluctuates around the freezing point seasonally. Over time, warming may expand the spatial extent of seasonal freeze and thaw, thereby increasing the thickness of the active layer. Consequently, the permafrost table would move downwards and more exchange of groundwater and surface water can be expected. The opposite would be expected with long-term cooling. These considerations require inclusion of permeability change with ice and water content, the latent heat process, as well as the advection of heat with flowing groundwater. SUTRA [*Voss and Provost*, 2004], a coupled fluid and heat transport model, was modified to incorporate a freeze and thaw dynamics by *McKenzie et al.* [2007]. The modified SUTRA code was used in this study. A brief summary of the main concepts of groundwater flow and heat transport in permafrost is provided below.

[7] Assuming fully saturated conditions, the driving forces for fluid flow in porous media include pressure and gravity [*Hubbert*, 1940]. A general form of Darcy's law for fluid flux in porous media can be expressed as [e.g., *Ingebritsen et al.*, 2006]:

$$q = -\frac{k\rho}{\mu}(\nabla P + \rho g \nabla Z) \tag{1}$$

where q is the Darcy flux [m/s], k is the permeability [m^2], ρ is fluid density [kg/m^3], μ is fluid viscosity [kg/(m·s)], P is pore pressure [kg/(m·s^2)], g is gravitational acceleration [m/s^2], and Z is the elevation of the point of interest [m]. Incorporating Darcy's Law into mass conservation gives the governing equation describing fluid flow in porous media:

$$\frac{\partial(n\rho)}{\partial t} = \nabla \cdot \left[-\frac{k\rho}{\mu}(\nabla P + \rho g \nabla Z)\right] \tag{2}$$

where n is porosity [1] and t is time [s]. Similarly, the governing equation for heat transport can be derived from Fourier's Law for heat conduction and energy conservation as follows [*McKenzie et al.*, 2007; *Bense et al.*, 2009]:

$$\nabla \cdot (K_m \nabla T) - C_f q \cdot \nabla T = C_m \frac{\partial T}{\partial t} + L \frac{\partial \theta}{\partial t} \tag{3}$$

where K_m is the thermal conductivity of medium [J/(s·m·°C)], T is temperature [°C], C_f is the heat capacity of water [J/(kg·°C)], C_m is the effective heat capacity of medium [J/(kg·°C)], L is the latent heat of fusion [J/kg], and θ is the liquid water content [1].

[8] Permeability in the permafrost region varies with liquid water and ice content. In general, permeability decreases with decreasing liquid water saturation, similar to what is known about permeability varying with water saturation in vadose zones. *Koopmans and Miller* [1966] showed how permeability varies with liquid saturation during freezing for various soils with further details on hysteresis for freeze and thaw cycles. Water saturation, S_w, can be computed by an empirical exponential relationship, $S_w = (1 - S_{wres})e^{-\left(\frac{T-T_L}{w}\right)^2} + S_{wres}$, where S_{wres} is the residual water saturation, T_L is the freezing point temperature, and w is a fitting parameter. The sum of ice saturation and water saturation is unity. The permeability can be computed by $k = k_s 10^{-\Omega(1-S_w)}$, where k_s is the saturated permeability, and Ω is an empirical impedance factor [*Hansson et al.*, 2004]. When the water saturation becomes 1, permeability is equal to saturated permeability for the unfrozen state. Liquid water saturation and relative permeability, k/k_s, reduce to their predefined minimum residual values as temperature drops below a predefined value (Table 1).

[9] The above approach, described in more detail by *McKenzie et al.* [2007], was implemented in this study and all parameters are listed in Table 1. Other approaches have been used to characterize permafrost permeability. For example, *Bense et al.* [2009] used an experiment-based relation between water saturation and relative permeability.

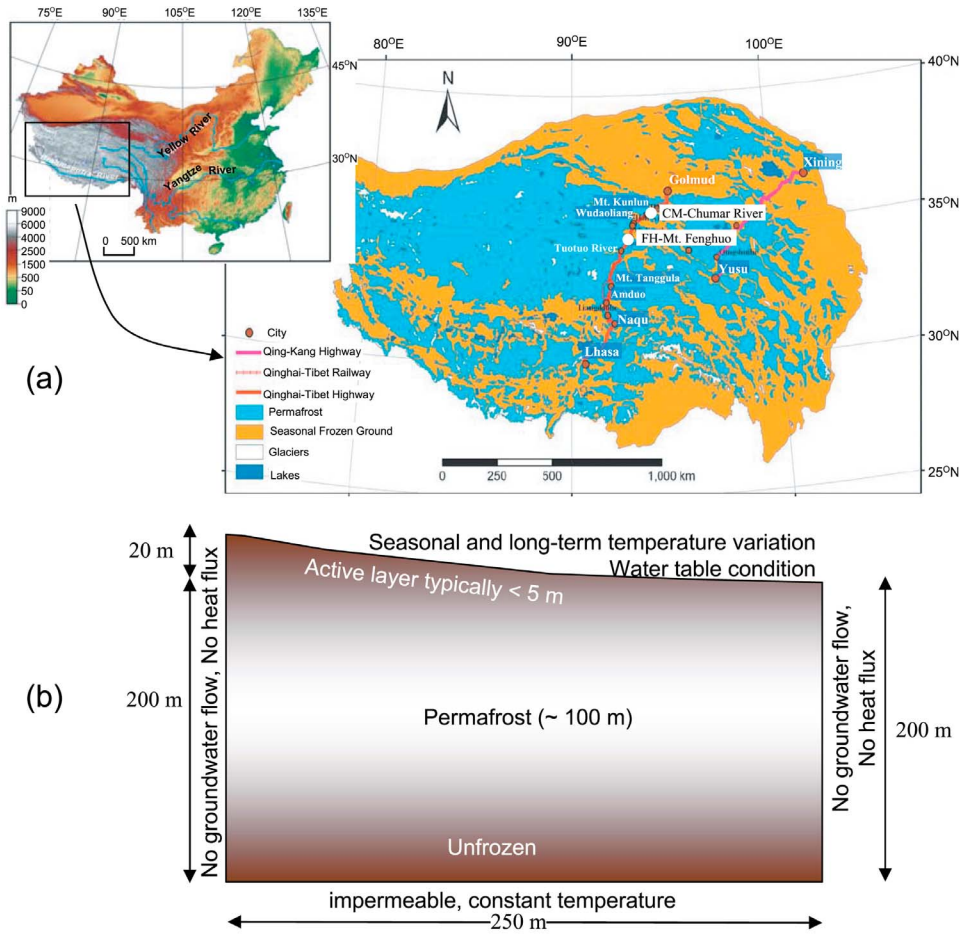

Figure 1. (a) Location of the Tibet Plateau, China [*Cheng and Wu*, 2007]. CM and FH are two sites along the Qinghai-Tibet Railroad where subsurface temperature data are used in this study. (b) A conceptual two-dimensional cross sectional model and boundary conditions for groundwater flow and heat transport, depicting a gentle hill slope on one side of a symmetric shallow and broad river valley. The color shade is not to scale, representing the active layer and permafrost that was formed in the geologic past.

3.2. Model Application to the Tibet Plateau, China

[10] The northern Tibet Plateau in China (Figure 1a) is underlain by continuous permafrost. A two-dimensional cross-sectional groundwater model, illustrated in Figure 1b, was developed to depict a gentle hill slope on one side of a symmetric shallow and broad river valley, representative of settings in the permafrost regions in northern central Tibet Plateau. The boundary conditions for groundwater flow are the following (Figure 1b): (1) No flow was assumed for the two lateral boundaries, approximating a topographic ridge and valley. (2) No flow was also assumed for the bottom, approximating low permeability bedrock at depth. (3) The top boundary coincides with the water table, where the pressure is specified as zero, equivalent to atmospheric pressure. For heat transport, the boundary conditions are: (1) Zero heat flux was assigned to the two lateral boundaries, consistent with the hydrogeologic conditions. (2) A constant temperature of 2°C was assigned at the bottom boundary, rather than a geothermal heat flux. Over the time scale of this study, flow processes in the active layer are limited to the upper 10 m. The bottom boundary at 200 m is sufficiently deep such that the processes in the active layer are not significantly affected by the conditions at this boundary (auxiliary material).[1] The specified temperature boundary condition was selected for simplicity. (3) The temperature at the land surface was approximated by a sinusoidal seasonal temperature variation. For simplicity, small magnitude temporal irregularities in air temperature (e.g., passing weather systems) are ignored and assumed to have a negligible effect on the subsurface thermal regime. Variations in daily air temperature and daily hours of bright sunshine can be important to the rate of landslide in permafrost regions [*Lewkowicz and Harris*, 2005].

[11] To obtain a dynamic steady state initial condition for subsequent simulations, the model was run for 30 years with the seasonally varied sinusoidal air temperature near the land surface. The results of the dynamic steady state background condition were compared with the temperature data from two sites, CM and FH (Figure 1a). The general site conditions are listed in Table 2. The temperature data were measured at various depths and averaged for each month over a ten-year period from 1996 to 2006 [*Wu and Zhang*,

[1]Auxiliary materials are available in the HTML. doi:10.1029/2011GL047911.

Table 2. Site Description[a]

Site Name	Altitude (m) Above Sea Level	Mean Annual Air Temperature (°C)	Mean Annual Ground Surface Temperature (°C)	Soil Conditions	Vegetation Cover, %	Active Layer Thickness (m)	Permafrost Thickness (m)
CM	4482	−5.5 to −5.0	−1.0 to −0.1	Sandy clay	20 to 30	2.5 to 4.0	10 to 30
FH	4938	−6.5 to −6.0	−3.0 to −2.0	Clay	70 to 80	1.5 to 2.5	80 to 120

[a]*Wu and Zhang* [2008].

2008]. The average air temperature is approximately 0°C at CM and −2.5°C at FH site. The amplitude of the approximate sinusoidal variation at both sites is near 10°C.

[12] A suite of simulations was conducted to calibrate the model. A permeability of 1×10^{-13} m^2 and porosity of 0.20 (Table 1) were found to produce simulated results that are most consistent with measured temperature data. These parameters are within the range of silt sands [*Freeze and Cherry*, 1979] and are consistent with previous hydrologic studies of the area [*Ge et al.*, 2008]. Figure 2 shows the comparison between modeled and measured temperatures at these two sites. Although discrepancies exist, modeled temperatures capture the major characteristics exhibited in the measured data and the overall patterns are in good agreement. Linear regression between measured and modeled temperature data yielded a fitting coefficient of 0.85 and R^2 value of 0.96 for the CM site and fitting coefficient of 0.89 and R^2 value of 0.93 for the FH site (auxiliary material).

[13] The latent heat effect is particularly noticeable at the CM site because the air temperature fluctuates around its average at the freezing point 0°C. As temperature increases in late spring and early summer to around zero, melting pore ice absorbs additional heat and slows the rate of temperature increase. Similarly, as temperature decreases in fall, freezing pore water releases latent heat and slows temperature decline. The latent heat effect at the FH site is less pronounced because of the below-freezing yearly average temperature. Only the upper most part of the active layer goes above the freezing point.

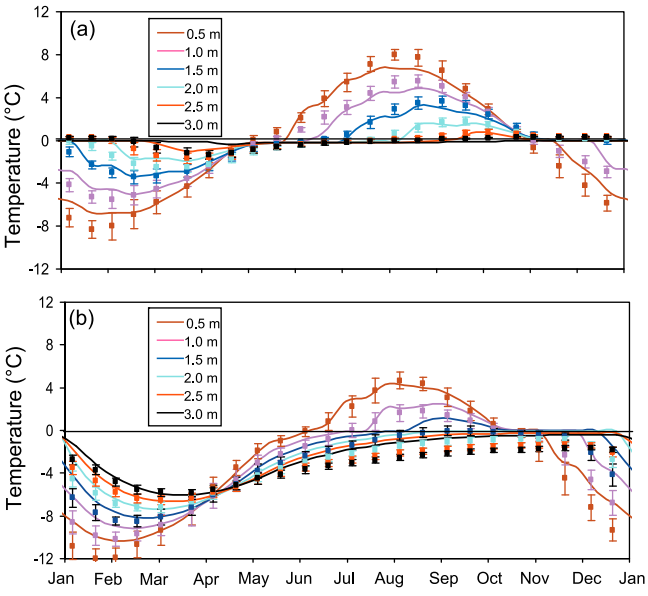

Figure 2. Comparison between modeled (lines) and measured (solid square symbols with error bars) temperatures at different depths. Measured data are averaged monthly temperatures from 1996 to 2005 at (a) CM site and (b) FH site. The error bars are the standard deviations for the measurement period. The non-smooth features (horizontal-trending) in the curves reflect the effects of latent heat.

4. Results

4.1. Seasonal Characteristics of Groundwater Discharge to Surface

[14] As the active layer goes through cycles of freezing and thawing, its permeability changes from nearly zero during most of the year to its maximum in summer. Consequently, groundwater discharge to the surface from the active layer occurs for five months during summer but is inactive the rest of the year. Using the parameters of the CM site, groundwater discharge response to the temperature change is illustrated in Figure 3. The discharge at a given time is obtained by integrating the flux across the top boundary. In a yearly cycle, from February to May, temperature rises but remains below zero. Therefore, the permeability is too low to allow groundwater flow and there is no discharge to the surface. In June, sufficient thawing allows permeability to increase and groundwater discharge occurs. This discharge continues to increase through the summer months, reaching a maximum in October, while subsurface temperatures are at their maxima in August (Figure 3). Groundwater flow starts to decrease in October as temperatures decline and becomes dormant from November to following April. As the hydrologic system goes through this annual cycle, heat transport is dominantly conductive from November to April but exhibits mixed conduction and advection from May to October. On the basis of Peclet number calculations, the advective fraction of total heat transport is 5% but can reach 28% in 40 years under the long-term warming scenario discussed in the next section.

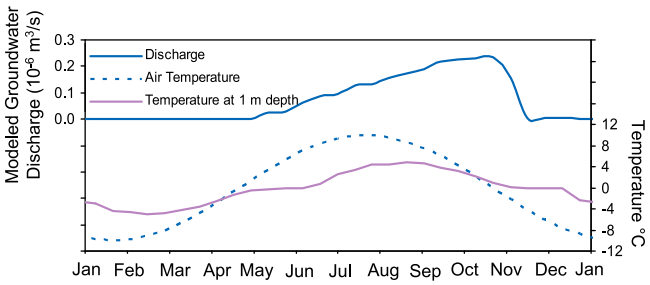

Figure 3. Modeled groundwater discharge in a 1-year cycle. Air temperature and modeled temperature at 1m depth are plotted for reference. The parameters used in modeling are listed in Table 1.

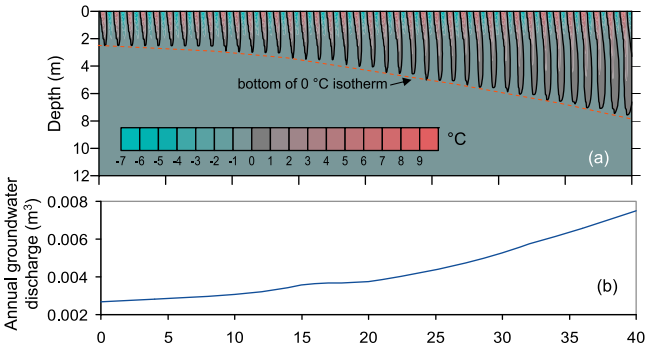

Figure 4. (a) Modeled temperature with depth over a period of 40 years under a temperature gradient of 3 °C/100 years. The blue and red bands represent freeze and thaw states of the active layer in yearly cycles. The solid lines are zero isotherms that approximate the lower boundary of the active layer. The change in active layer thickness can be inferred by the maximum depth of the zero isotherms (red dashed line). (b) Corresponding groundwater discharge to surface. The parameters used in modeling are for the CM site and listed in Table 1.

[15] Groundwater discharge was upscaled by the approximate catchment area of 200 m valley width by 500 km river length and compared to measured flow in the Chumar River near the CM site. Groundwater discharge peaks at the same time as river flows, and groundwater discharge comprises up to 9% of mean annual river flow (auxiliary material).

4.2. Decadal Variations in Active Layer Thickness and Groundwater Discharge

[16] To investigate the long term impact of increasing mean air temperature on permafrost and near surface hydrology, an increase of 3°C per 100 years in the mean yearly temperature was superimposed on the seasonal temperature variation. The dynamic steady state condition under seasonal temperature variation was used as the initial condition. Figure 4a shows the temperature variation with depth at the middle section of the hill slope over a 40 year period. The modeled active layer thickness increases by a factor of three from 2.5 m to 7.6 m, as shown by the warm color zones in Figure 4a. The increasing trend is illustrated by the dashed line that connects the maximum depth of the active layer in each year. Corresponding long term groundwater discharge is shown in Figure 4b. As the active layer thickness increases, its permeability is increased, which leads to increased groundwater discharge. An increase of three-fold in groundwater discharge over 40 years is predicted (Figure 4b). This increase is consistent with the early time trend of the long-term groundwater discharge modeled by *Bense et al.* [2009].

5. Summary and Conclusions

[17] This modeling study couples fluid flow and heat transport to examine the response of groundwater flow in the permafrost active layer to air temperature variations. The model incorporates conductive and advective heat transport, latent heat released or absorbed during freezing and thawing, permeability variation as a function of ice-water saturation, as well as seasonal and long-term temperature variations.

[18] The model results show that the subsurface temperatures in the uppermost few meters of the permafrost region respond to a simple sinusoidal air temperature variation with a lag of approximately one month (Figure 3). In a yearly cycle, groundwater flow occurs in the active layer for five months. In the case of northern central Tibet Plateau, the groundwater discharge period is from May to October. Maximum groundwater discharge lags the maximum subsurface temperature by approximately two months (Figure 3).

[19] Under a scenario of temperature increasing by 3°C per 100 years over a period of 40 years, the active layer thickness can increase by three-fold during the first 40 years. In the northern central Tibet Plateau, the active layer is predicted to increase from 2.5 m to 7.6 m. and groundwater discharge to surface is predicted to increase by three-fold.

[20] These results imply that with increased warming there will be more groundwater flow in the active layer and therefore increased groundwater discharge to rivers. However, this finding only holds if sufficient upgradient water is available to replenish the shallow groundwater system that undergoes increased discharge. Otherwise, there will be an overall lowering of the water table in the recharge portion of the catchment. The increased groundwater flow in the active layer could promote nutrient transport or mobilize previously stationary chemical constituents in shallow soils.

[21] **Acknowledgments.** The authors thank Ean Warren, Helen French, two anonymous reviewers, and Editor Paolo D'Odorico for their valuable comments. SG acknowledges the support from National Science Foundation grant CMG 0934647. QBW thanks the State Key Science Research Program for Global Change Research of China (grant 2010CB951402).

[22] The Editor thanks the two anonymous reviewers for their assistance in evaluating this paper.

References

Bense, V. F., G. Ferguson, and H. Kooi (2009), Evolution of shallow groundwater flow systems in areas of degrading Permafrost, *Geophys. Res. Lett.*, *36*, L22401, doi:10.1029/2009GL039225.

Bockheim, J.-G. (1995), Permafrost distribution in the southern circumpolar region and its relationship to the environment: A review and recommendations for further research, *Permafrost Periglacial Processes*, *6*, 27–45, doi:10.1002/ppp.3430060105.

Cheng, G., and T. Wu (2007), Responses of permafrost to climate change and their environmental, significance, Qinghai-Tibet Plateau, *J. Geophys. Res.*, *112*, F02S03, doi:10.1029/2006JF000631.

Freeze, A. R., and J. Cherry (1979), *Groundwater*, Prentice Hall, Englewood Cliffs, N. J.

Frey, K. E., D. I. Siegel, and L. C. Smith (2007), Geochemistry of west Siberian streams and their potential response to permafrost degradation, *Water Resour. Res.*, *43*, W03406, doi:10.1029/2006WR004902.

Ge, S., Q. B. Wu, N. Lu, G. L. Jiang, and L. Ball (2008), Groundwater in the Tibet Plateau, western China, *Geophys. Res. Lett.*, *35*, L18403, doi:10.1029/2008GL034809.

Hansson, K., J. Simunek, M. Mizoguchi, L.-C. Lundin, and M. T. Genuchten (2004), Water flow and heat transport in frozen soil: Numerical solution and freeze–thaw applications applied, *Vadose Zone J.*, *3*, 693–704, doi:10.2113/3.2.693.

Hinzman, L. D., D. L. Kane, R. E. Gieck, and K. R. Everett (1991), Hydrologic and thermal properties of the active layer in the Alaskan Arctic, *Cold Reg. Sci. Technol.*, *19*, 95–110, doi:10.1016/0165-232X(91)90001-W.

Hubbert, K. (1940), The theory of ground-water motion, *J. Geol.*, *48*(8), 785–944, doi:10.1086/624930.

Ingebritsen, S., W. Sanford, and C. Neuzil (2006), *Groundwater in Geologic Processes*, Cambridge Univ. Press, Cambridge, U. K.

Koopmans, R. W. R., and R. D. Miller (1966), Soil freezing and soil water characteristic curves, *Soil Sci. Soc. Am. J.*, *30*, 680–685, doi:10.2136/sssaj1966.03615995003000060011x.

Lewkowicz, A. G., and C. Harris (2005), Frequency and magnitude of active-layer detachment failures in discontinuous and continuous permafrost, northern Canada, *Permafrost Periglacial Processes*, *16*, 115–130, doi:10.1002/ppp.522.

Liu, J., N. Hayakawa, M. Lu, S. Dong, and J. Yuan (2003), Winter streamflow, ground temperature and active-layer thickness in northeast China, *Permafrost Periglacial Processes*, *14*, 11–18, doi:10.1002/ppp.436.

McKenzie, J., C. Voss, and D. Seigel (2007), Groundwater flow with energy transport and water–ice phase change: Numerical simulations, benchmarks, and application to freezing in peat bogs, *Adv. Water Resour.*, *30*, 966–983, doi:10.1016/j.advwatres.2006.08.008.

Michel, F. A. (1994), Changes in hydrogeological regimes in permafrost regions due to climate change, *Permafrost Periglacial Processes*, *5*, 191–195, doi:10.1002/ppp.3430050308.

Person, M., J. Raffensperger, S. Ge, and G. Garven (1996), Basin-scale hydrological modeling, *Rev. Geophys.*, *34*(1), 61–78, doi:10.1029/95RG03286.

Smith, S. L., V. E. Romanovsky, A. G. Lewkowicz, C. R. Burn, M. Allard, G. D. Clow, K. Yoshikawa, and J. Throop (2010), Thermal state of permafrost in North America: A contribution to the International Polar Year, *Permafrost Periglacial Processes*, *21*, 117–135, doi:10.1002/ppp.690.

St. Jacques, J.-M., and D. J. Sauchyn (2009), Increasing winter baseflow and mean annual streamflow from possible permafrost thawing in the Northwest Territories, Canada, *Geophys. Res. Lett.*, *36*, L01401, doi:10.1029/2008GL035822.

Thomas, H. R., P. Cleall, Y.-C. Li, C. Harris, and M. Kern-Luetschg (2009), Modelling of cryogenic processes in permafrost and seasonally frozen soils, *Geotechnique*, *59*(3), 173–184, doi:10.1680/geot.2009.59.3.173.

Voss, C., and A. Provost 2004, SUTRA, a model for saturated-unsaturated variable-density ground-water flow with solute or energy transport, *U.S. Geol. Surv. Water Resour. Invest. Rep., 02-4231.*

Walvoord, M. A., and R. G. Striegl (2007), Increased groundwater to stream discharge from permafrost thawing in the Yukon River basin: Potential impacts on lateral export of carbon and nitrogen, *Geophys. Res. Lett.*, *34*, L12402, doi:10.1029/2007GL030216.

Wu, Q., and T. Zhang (2008), Recent permafrost warming on the Qinghai-Tibetan Plateau, *J. Geophys. Res.*, *113*, D13108, doi:10.1029/2007JD009539.

Yang, D., D. L. Kane, L. D. Hinzman, X. Zhang, and T. Zhang (2002), Siberian Lena River hydrologic regime and recent change, *J. Geophys. Res.*, *107*(D23), 4694, doi:10.1029/2002JD002542.

Zarnetske, J. P., M. N. Gooseff, W. B. Bowden, M. J. Greenwald, T. R. Brosten, J. H. Bradford, and J. P. McNamara (2008), Influence of morphology and permafrost dynamics on hyporheic exchange in arctic headwater streams under warming climate conditions, *Geophys. Res. Lett.*, *35*, L02501, doi:10.1029/2007GL032049.

Zhang, T., R. G. Barry, K. Knowles, F. Ling, and R. L. Armstrong (2003), Distribution of seasonally and perennially frozen ground in the Northern Hemisphere, in *Permafrost*, edited by M. Phillips et al., pp. 1289–1294, Swets and Zeitlinger, Amsterdam.

Zhao, L., Q. Wu, S. S. Marchenko, and N. Sharkhuu (2010), Thermal state of permafrost and active layer in central Asia during the International Polar Year, *Permafrost Periglacial Processes*, *21*, 198–207, doi:10.1002/ppp.688.

S. Ge, Department of Geological Sciences, University of Colorado at Boulder, Campus Box 399, Boulder, CO 80309, USA. (ges@colorado.edu)

J. McKenzie, Earth and Planetary Sciences, McGill University, 3450 University St., Montreal, QC H3A 2A7, Canada.

C. Voss, U.S. Geological Survey, 345 Middlefield Rd., Menlo Park, CA 94025, USA.

Q. Wu, State Key Laboratory of Frozen Soil Engineering, Cold and Arid Regions Environmental and Engineering Research Institute, Chinese Academy of Sciences, Lanzhou 730000, China.